



# Mathematical Modeling of the Flow of Viscous Incompressible Fluid with Suspended Particles in Flat Inclined Channel

Regina Iulmukhametova<sup>(✉)</sup>, Airat Musin, and Liana Kovaleva

Bashkir State University, Ufa, Russian Federation

**Abstract.** In this paper, we simulate the flow of a disperse system, consisting of solid spherical particles and viscous incompressible fluid, in a flat channel at different angles of inclination. The mathematical model written in the one-fluid approximation includes the equation of continuity for mixture, the equation of motion of the mixture, and the balance equation in the form of a convective-diffusion equation for the transfer of the volume concentration of particles. The system of equations of the mathematical model was solved with the control volume method in the OpenFoam software package. It was found that the limiting liquid injection rate into the channel, at which the channel is filled with a solid phase, depends on the angle of inclination according to the harmonic law.

**Keywords:** Disperse system · Single-fluid approximation · Suspension flow · Solid particles · Flat inclined channel

## 1 Introduction

A flow of suspensions in the channel is found in many areas of industry. For example, when applying one of the most popular stimulation technologies - hydraulic fracturing. The issue of transporting proppant in a fracture is associated with gravitational deposition of proppant, using the correct fluid to transport it deep into the fracture, leakage of fluid from the fracture to the formation, and plugging of the fractures [1]. However, despite their widespread use, the properties of suspensions still can't be properly predicted using a single numerical model. In the case where the suspension contains particles with a density higher than liquid, they tend to settle and accumulate along the length of the channel. When working with such suspensions, it is necessary to take into account many variables, such as flow characteristics, flow behavior in channels of various geometries, as well as particle concentration, shape, size, and size distribution [2]. For concentrated suspensions, during numerical modeling, it is also important to take into account phenomena such as the interaction between particles, between particles and walls, particle migration, flow regime, as well as lifting forces.

Considering approaches to modeling the flow of suspensions, two approaches can be distinguished: single-fluid and two-continuum [3–5]. The differences between the one-liquid model and the two-continuum model are significant. However, for most practical purposes, solving a complete system of two-continuum models not only requires computational costs but is also not necessary. The authors of [5] noted that when stable flows are characterized by a short dynamic particle relaxation time compared to hydrodynamic time or a small Stokes number, particle transport has a diffusion character. The diffusion model of the suspension is applicable for modeling various laminar flows of the suspension in the Stokes approximation.

## 2 Numerical Research

### 2.1 Problem Statement

We study the flow of viscous incompressible fluid with suspended solid spherical particles in flat inclined channel. It is believed that the fluid is incompressible, solid spherical particles have the same size and shape, flow is laminar. Figure 1 shows a schematic of the computational domain.

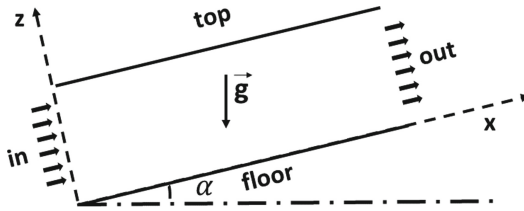


Fig. 1. Computational domain

### 2.2 Mathematical Model

The mathematical model written in the one-fluid approximation, includes the equation of continuity for mixture, equation of motion of the mixture, the balance equation in the form of a convective-diffusion equation for the transfer of the volume concentration of particles [5,6]:

$$\frac{\partial \rho}{\partial t} + \nabla \cdot (\rho \mathbf{u}) = 0 \quad (1)$$

$$\frac{\partial(\rho \mathbf{u})}{\partial t} + \nabla \cdot (\rho \mathbf{u} \mathbf{u}) = -\nabla p + \rho \mathbf{g} + \nabla \cdot \Sigma - \nabla \cdot \left( \frac{\rho_p \rho_f}{\rho} (1 - C) C \mathbf{u}_r \mathbf{u}_r \right) \quad (2)$$

$$\frac{\partial C}{\partial t} + \nabla \cdot (C\mathbf{u}) = -\nabla \cdot (C(1 - f_p)\mathbf{u}_r) \quad (3)$$

where  $\rho = \rho_p C + \rho_f(1 - C)$  – mixture density;  $\mathbf{u}$  – mixture velocity;  $p$  – average mixture pressure;  $C$  – volume concentration;  $f_p = \rho_p C / \rho$  – mass fraction of dispersed phase;  $\mathbf{g} = (-g \sin \alpha, 0, -g \cos \alpha)$  – gravity acceleration;  $\alpha$  – angle of inclination;  $\Sigma = \mu[\nabla \mathbf{u} + (\nabla \mathbf{u})^T - 2/3(\nabla \cdot \mathbf{u})I]$  – stress tensor in mixture;  $\mathbf{u}_r$  – relative velocity between phases;  $\mu$  – effective viscosity ratio of the mixture;  $I$  – identity matrix. Hereinafter index  $p$  denotes parameters related to solid dispersed phase,  $f$  – to liquid continuous phase.

The coefficient of effective viscosity of the mixture is calculated according to the empirical relationship proposed by Krieger [7]:

$$\mu = \mu_f \left(1 - \frac{C}{C_{max}}\right)^{-\beta} \quad (4)$$

where  $\mu_f$  – dynamic viscosity coefficient of liquid continuous phase;  $C_{max}$  – ultimate packing density of particles;  $\beta$  – empirical coefficient.

Relative velocity between phases is determined by the formula [5]:

$$\mathbf{u}_r = f^h(\mathbf{u}_{st} - \frac{d^2(\rho_p - \rho_f)}{18\mu_f} \frac{d\mathbf{u}}{dt} + \frac{d^2}{18\mu_f C} \nabla \cdot \Sigma_p) \quad (5)$$

$$\mathbf{u}_{st} = \frac{d^2(\rho_p - \rho_f)\mathbf{g}}{18\mu_f} \quad (6)$$

$$\nabla \cdot \Sigma_p = -\gamma \nabla(\mu_f a_n) - K_\gamma \mu_f a_n \nabla \gamma \quad (7)$$

$$K_\gamma = \left(2 - \frac{K_\eta}{K_c}\right) \left(1 - \frac{C}{C_{max}}\right)^p + \frac{K_\eta}{K_c} \quad (8)$$

where  $\mathbf{u}_{st}$  – sedimentation velocity according to Stokes;  $d$  – particle diameter;  $\Sigma_p$  – stress tensor in the medium of particles;  $\gamma$  – mixture flow shear rate;  $a_n = \mu/\mu_f - (1 + 2.5C)$  – empirical function;  $K_c$  and  $K_\eta$  – empirical coefficients, the ratio of which according to [8] is defined as  $K_c/K_\eta = 1.042C + 0.1142$ .

The constrained sedimentation function is determined by the formula:

$$f^h = \left(1 - \left(\frac{C}{C_{max}}\right)^2\right) \left(1 - \frac{C}{C_{max}}\right)^\beta \quad (9)$$

Initial conditions:

$$C(x, y, z, t = 0) = 0 \quad (10)$$

$$\mathbf{u}(x, y, z, t = 0) = 0 \quad (11)$$

Boundary conditions

For the volume concentration on solid walls, the condition of the absence of flow into the wall is set:

$$\frac{\partial C}{\partial n} = 0 \quad (12)$$

A constant concentration at the channel entrance  $C_{in}$  is set:

$$C(x, y, z, t = 0) = C_{in} \quad (13)$$

At the exit from the channel, a flow condition is specified.

For the tangent component of the mixture velocity to the wall, the condition of partial slip on the wall is specified [5]:

$$\beta_w d \left( 1 - \frac{C}{C_{max}} \right) C \frac{\mu}{\mu_f} \frac{\partial u}{\partial n} = u \quad (14)$$

where  $\beta_w$  – slip parameter depending on the sphere radius [9].

For the normal component of the mixture velocity to the wall, the no-flow condition on the solid wall is specified:

$$\mathbf{u}_{n_w} = 0 \quad (15)$$

where  $\mathbf{n}_w$  – normal to the wall surface.

Constant velocity at the entrance to the channel:

$$\mathbf{u} = (u_{in}, 0, 0) \quad (16)$$

At the exit from the channel, the flow condition is set:

$$\frac{\partial \mathbf{u}}{\partial n} = 0 \quad (17)$$

### 3 Results

The problem in the three-dimensional formulation was solved numerically in an open-source CFD software OpenFOAM using the control volume method.

To validate the program code, we compared the calculation results with experimental data [10]. The authors of the experiment studied fully developed profiles of particle velocity and concentration during suspension flow in a flat channel. Satisfactory agreement between results of numerical calculation and experiment was obtained.

The results of the numerical simulation were obtained with the following system parameters: channel length – 0.5 m, width – 0.002 m, height – 0.04 m,  $\rho_f = 1000 \text{ kg/m}^3$ ,  $\mu_f = 0.001 \text{ Pa} \times \text{s}$ ,  $\rho_p = 2650 \text{ kg/m}^3$ ,  $d = 0.0004 \text{ m}$ ,  $C_{in} = 0.3$ ,  $C_{max} = 0.64$ , parameter  $p = 8$ ,  $\beta = 1.4$ .

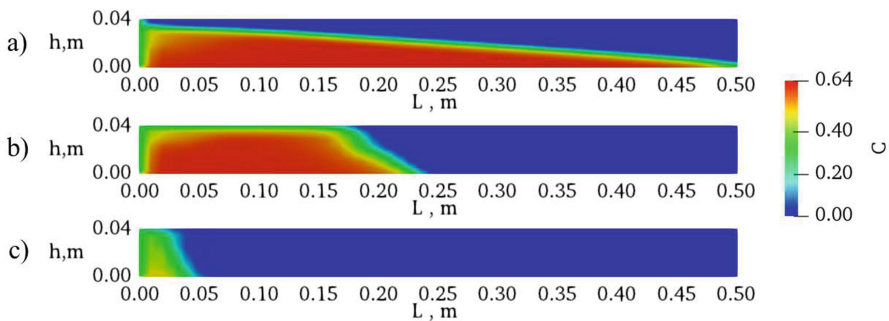
Comparative modeling of the distribution dynamics of the solid spherical particles concentration the fluid flow and their sedimentation along the channel,

depending on the fluid injection rate ( $u_{in}$ ) and the angle of inclination of the channel relative to the horizon ( $\alpha$ ) (Fig. 1), has been carried out.

The value of the liquid injection rate into the channel was chosen so that the flow rate in the channel was comparable to the Stokes sedimentation rate (6). The channel tilt angle varied from 0 to  $\pi/2$ . The tilt angle 0 corresponds to the case when the injection velocity vector is perpendicular to the gravity vector, and the tilt angle  $\pi/2$  corresponds to the case when these vectors are oppositely directed.

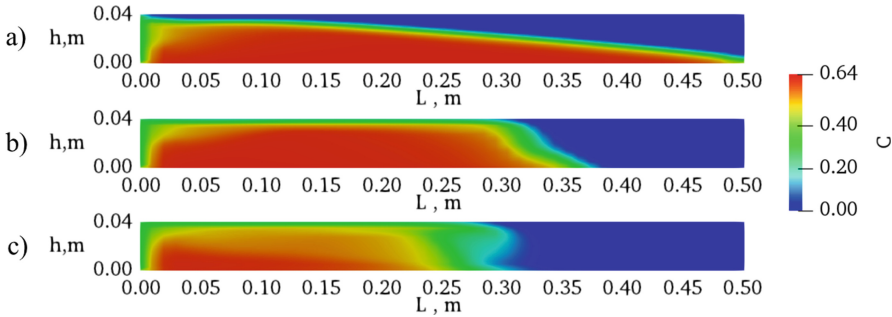
The simulation showed that at low injection rate the fluid in the channel at a certain non-zero angle of inclination the particles stop moving along the channel, which is associated with excess gravitational particle sedimentation rate on the flow rate of the mixture.

Figure 2 shows the graphs of the distribution of the concentration of solid spherical particles along the center of the channel at an injection rate of  $u_{in} = 0.02$  m/s at tilt angles a) 0, b)  $\pi/6$  and c)  $\pi/3$ , plotted at the time  $t = 40$  s. It can be seen from the figure that in the horizontal channel (Fig. 2a) during this time the particles reach the end of the channel. The height of the formed sediment decreases almost linearly from the entrance to the channel to its exit and practically doesn't change over time. At the channel tilt angle  $\pi/6$ , a different picture is observed (Fig. 2b). The left part of the channel is almost completely occupied by the sediment; during this time, the particle front reaches only the middle of the channel. This is because this injection rate is comparable to the sedimentation rate of particles and the particles hardly overcome gravitational forces. In the left part of the channel, an area with a low concentration of particles, in which liquid movement is possible, is observed only in the near-wall region in the upper part of the channel. In the lower part, the concentration is close to the limit value of close packing. With an increase in the channel tilt angle to  $\pi/3$  (Fig. 2c), the situation is aggravated. During the considered time, the particles have time to overcome only a small part of the path and accumulate at the entrance to the channel.



**Fig. 2.** Distribution of concentration of solid particles along the length of the channel at  $u_{in} = 0.02$  m/s at an angle of inclination: a - 0; b -  $\pi/6$ ; c -  $\pi/3$ ;

At higher injection rates, the pattern of sediment distribution in the channel changes significantly. Figure 3 shows the graphs of the distribution of the concentration of solid spherical particles along the center of the channel at different angles of inclination of the channel at an injection rate of 0.04 m/s, which is twice the value of the rate at which the previous results were obtained. Accordingly, the time at which the distributions were plotted was chosen two times less and is  $t = 20$  s. It can be seen that in the horizontal channel the pattern of sediment distribution along the channel (Fig. 3a) practically doesn't differ from the results obtained at a lower injection rate (Fig. 2a). The height of the formed sediment decreases almost linearly from the entrance to the channel to its exit. At an angle of inclination of the channel  $\pi/6$ , the pattern of the sediment distribution (Fig. 3b) is also identical to the pattern obtained at a lower velocity (Fig. 2b). However, at large tilt angles of the channel ( $\pi/3$ ), a significantly different picture of the sediment distribution is observed (Fig. 3c). In the lower part of the channel, a small area with sediment is formed, the concentration of which is close to the limiting one. The area of low concentration in the upper part of the channel is wider than at lower tilt angles. In this case, the displacement front in this case slightly lags behind the front at an angle of  $\pi/6$  and reaches almost the middle of the channel (Fig. 3c), which is much further than at an injection rate of 0.02 m/s (Fig. 2c).



**Fig. 3.** Distribution of concentration of solid particles along the length of the channel at  $u_{in} = 0.04$  m/s at an angle of inclination: a - 0; b -  $\pi/6$ ; c -  $\pi/3$ ;

This is due to the fact that the flow rate in the channel is much higher than the rate of gravitational sedimentation of particles. In addition, in this case, a significant blurring of the displacement front is observed. The structure of the front has the shape of an incident wave; in the upper and lower parts of the channel, the front of particles leads the front in the middle of the channel.

For clarity, Fig. 4 shows the concentration distribution along the channel in the upper, lower and middle parts of the channel, plotted for the tilt angles  $\pi/6$  and  $\pi/3$  at an injection rate of 0.04 m/s. It is seen that at an angle of  $\pi/6$ , the front of particles in the lower part of the channel leads the front in the middle and upper parts, and at an angle of  $\pi/3$ , the front in the upper part of the

channel begins to lead. This is due to the fact that at high velocities with an increase in the angle of inclination of the channel behind the displacement front, a vortex flow of the liquid arises, which increases with an increase in the injection rate.

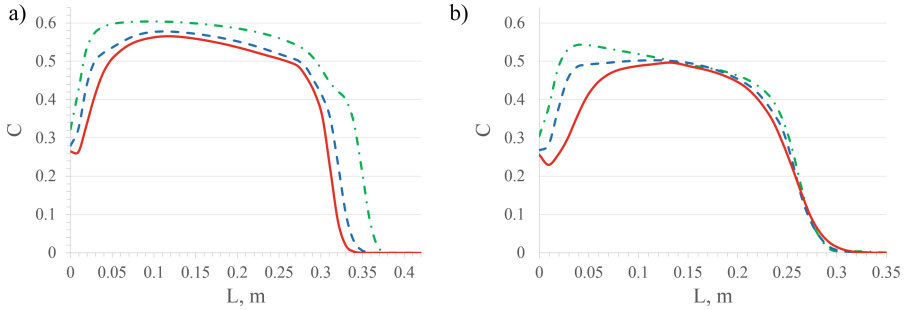


**Fig. 4.** Concentration distribution along the channel in the upper (line), lower (dashed line with dot) and middle (dashed line) parts of the channel at  $u_{in} = 0.04$  m/s at an angle of inclination: a -  $\pi/6$ ; b -  $\pi/3$ ;

Figure 5 shows the velocity field and streamlines in the channel at different slope angles ( $0$ ,  $\pi/6$  and  $\pi/3$ ) at an injection rate of  $0.04$  m/s, which corresponds to the concentration distribution pattern in Fig. 3.

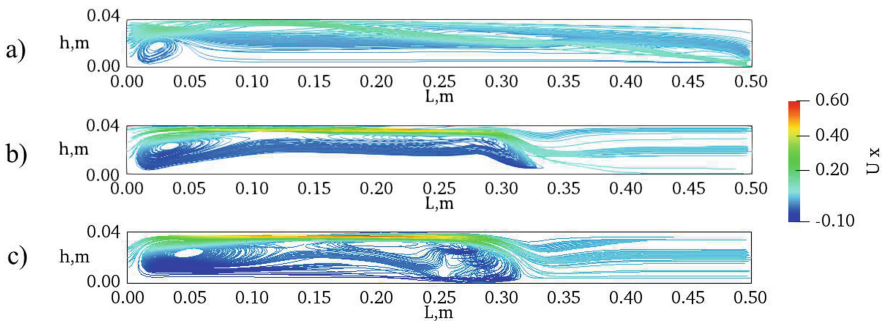


**Fig. 5.** Velocity field and streamlines for  $u_{in} = 0.04$  m/s at an angle of inclination: a -  $0$ ; b -  $\pi/6$ ; c -  $\pi/3$ ;

It can be seen that in the horizontal channel (Fig. 5a) streamlines are directed mainly along the channel. The vortex flow occurs only at the entrance to the channel due to the formation of a particle roll and doesn't have a strong effect on the formation of the particle front in the depth of the channel. With an increase in the depth of the channel up to  $\pi/6$  (Fig. 5b), the size of the vortex arising at the entrance to the channel increases.

The flow velocity of the mixture in the upper part of the channel becomes noticeably higher than in the rest of the channel due to the formation of a layer with a dense packing of particles, in which there is practically no movement. At an angle of inclination  $\pi/3$ , the vorticity of the flow behind the displacement front is observed, which leads to the blurring of the front, which is observed in Fig. 3c.

During computational studies, it was found that the limiting rate of liquid injection into the channel at which the channel begins to fill with a solid phase depends on the angle of inclination according to the harmonic law and is described by the following equation:

$$u_{in} = u_{\pi/2} \cdot \sin(\alpha) \quad (18)$$

where  $u_{\pi/2}$  is the limiting velocity at which the filling of the channel with a solid phase begins for the angle  $\pi/2$ .

Figure 6 shows this dependence. It can be seen that with an increase in the angle of inclination, the limiting velocity increases and has a maximum value at an angle  $\pi/2$ , which corresponds to the movement of the liquid against the action of gravity. Since the channel is symmetric about the center, it is quite obvious that the curve in Fig. 6 can be extended symmetrically to the angle  $\pi$ . The part of the curve from  $\pi/2$  to  $\pi$  will be described by the same dependence and correspond to the channel tilt to the other side.

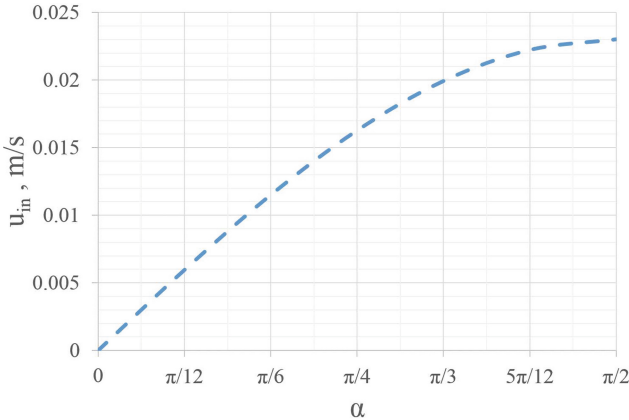


**Fig. 6.** Dependence of the limiting liquid injection rate into the channel at which the channel starts filling with the solid phase on the channel tilt angle

## 4 Conclusion

The mathematical model of the laminar flow for incompressible fluid with suspended particles in the one-fluid approximation in the Open Foam software

package was implemented. The algorithm has been tested on experimental data. Satisfactory agreement between results of numerical calculation and experiment was obtained.

The study of the particles distribution dynamics in the fluid flow, as well as their sedimentation along the length of the channel, depending on the values of the fluid injection rate and the angle of inclination of the channel relative to the horizon was carried out.

It is shown that at a high injection rate in a horizontal channel, the vortex flow arising at the entrance to the channel doesn't have a strong effect on the formation of the front of particles in the depth of the channel. With an increase in the angle of inclination to  $\pi/6$ , the size of the vortex flow arising at the entrance of the channel increases. The flow rate of the mixture in the top of the channel becomes noticeably higher than in the rest of the channel where, due to the formation of a layer with a dense packing of particles, their movement is practically absent. When an angle of inclination equal to  $\pi/3$ , a vorticity of the flow behind the displacement front appears, which leads to a blurring of the front.

It was found that at a low rate of liquid injection into the channel at a certain non-zero angle, the particles cease to move along the channel, which is associated with the excess of the gravitational sedimentation of particles over the mixture flow rate.

It was also found that the limiting liquid injection rate into the channel, at which the channel is filled with a solid phase, depends on the angle of inclination according to the harmonic law.

**Acknowledgments.** The reported study was funded by RFBR, project number 19-31-90157.

## References

1. Aksakov, A.V., et al.: Corporate fracturing simulator: from a mathematical model to software implementation. *Oil Ind.* **11**, 35–40 (2016). (in Russian)
2. Sokovnin O.M., Zagoskin N.V., Zagoskin S.N. Hydrodynamics of Motion of Particles, Droplets and Bubbles in Non-Newtonian Fluids, p. 215. Nauka (2019). (in Russian)
3. Nigmatulin, R.I.: Dynamics of Multiphase Media, vol. I and II, p. 464. Nauka, Moscow (1987)
4. Boronin, S.A., Osipov, A.A.: Two-continuous model of a suspension flow in a hydraulic fracture. *Rep. Acad. Sci.* **431**(6), 758–761 (2010). (in Russian)
5. Gavrillov, A.A., Shebelev, A.V.: Single-fluid model of a mixture for laminar flows of highly concentrated suspensions. *Fluid Dyn.* **53**(2), 255–269 (2018)
6. Manninen, M., Taivassalo, V., Kallio, S.: On the mixture model for multiphase flow, p. 67. VTT Publications 288. Technical Research Centre of Finland (1996)
7. Krieger, I.M.: Rheology of monodisperse lattice. *Adv. Colloid Interface Sci.* **3**, 111–136 (1972)
8. Tetlow, N., Graham, A.L., Ingber, M.S., Subia, S.R., Mondy, L.A., Altobelli, S.A.: Particle migration in a Couette apparatus: experiment and modeling. *J. Rheol.* **42**, 307–327 (1998)

9. Ingber, M.S., Graham, A.L., Mondy, L.A., Fang, Z.: An improved constitutive model for concentrated suspensions accounting for shear-induced particle migration rate dependence on particle radius. *Int. J. Multiph. Flow* **35**, 270–276 (2009)
10. Lyon, M.K., Leal, L.G.: An experimental study of the motion of concentrated suspensions in two-dimensional channel flow. Part 1 monodisperse systems. *J. Fluid Mech.* **363**, 25–56 (1998)